The Variable Twist of Actin and Its Modulation by Actin-binding Proteins

David L. Stokes* and David J. DeRosier‡

*Graduate Program in Biophysics, and ‡Department of Biology, Rosenstiel Basic Medical Sciences Research Center, Brandeis University, Waltham, Massachusetts 02254

Abstract. Previous studies demonstrated that actin filaments have variable twist in which the intersubunit angles vary by $\sim\pm10°$ within a filament. In this work we show that this variability was unchanged when different methods were used to prepare filaments for electron microscopy. We also show that actin-binding proteins can modulate the variability in twist.

Three preparations of actin filaments were photographed in the electron microscope: negatively stained filaments, replicas of rapidly frozen, etched filaments, and frozen hydrated filaments. In addition, micrographs of actin + tropomyosin + troponin (thin filaments), of actin + myosin S1 (decorated filaments), and of filaments frayed from the acrosomal process of *Limulus* sperm (*Limulus* filaments) were obtained. We used two independent methods to measure variable twist based on Fourier transforms of single filaments. The first involved measuring layer line intensity versus filament length and the second involved measuring layer line position. We measured a variability in the intersubunit angle of actin filaments of $\sim12°$ independent of the method of preparation or of measurement. Thin filaments have 15° of variability, but the increase over pure actin is not statistically significant. Decorated filaments and *Limulus* filaments, however, have significantly less variability (~2 and 1°, respectively), indicating a torsional stiffening relative to actin. The results from actin alone using different preparative methods are evidence that variable twist is a property of actin in solution. The results from actin filaments in the presence of actin-binding proteins suggest that the angular variability can be modulated, depending on the biological function.

ACTIN is one of the main structural proteins available to the cell; actin and various actin-binding proteins combine to form both motile and nonmotile assemblies. The widespread occurrence of these assemblies in the cell has generated interest in the structural properties of actin filaments and in the modulation of these properties by actin-binding proteins. A variability in the twist of actin filaments is a property that appears to be important in the construction of actin assemblies. We report here both on measurements of the variable twist of actin and on the effect of actin-binding proteins on this variability.

The formation of bonds that hold bundles of actin filaments together seems to require filaments that can be locally twisted, thereby perturbing the underlying helical symmetry. For example, in bundles found both in microvilli and in stereocilia, bonds are formed along a hexagonal packing lattice between filaments that do not have hexagonal symmetry. To make interfilament crossbridges at 60° intervals, positions of actin subunits must be rotated by as much as 7° (DeRosier and Censullo, 1981). A local change in twist of actin filaments thus permits the hexagonal cross-bridging needed for bundle formation. In striated muscle the geometry is more complicated, since actin's symmetry matches neither the hexagonal packing lattice nor the helical symmetry of the myosin thick filaments (Huxley and Brown, 1967). Again, flexibility is required to make cross-bridges and in this case to develop tension, but the necessary flexibility could come from either actin, myosin, or both. Indeed, the formation of cross-bridges during rigor appears to induce distortions, as seen in three-dimensional reconstructions of insect flight muscle (Taylor et al., 1984). The distinct angular distortions of actin filaments in these reconstructions suggest that local twisting of actin plays some role in the actin–myosin interaction. The extent of these distortions is consistent with $\sim15°$ of rotational freedom for each actin subunit relative to its neighbors in the filament (Egelman, 1985).

There are two types of evidence for the variability in twist of isolated actin filaments. Spectroscopic measurements offer evidence for dynamic twisting of individual filaments in solution. Mobilities with time constants of 0.1 ms have been observed and assigned to a torsional motion of individual filaments in solution (Thomas et al., 1979; Yoshimura et al., 1984). Also, a variability in the twist of filaments has been directly observed in the electron microscope. While spectroscopy tends to measure the time-averaged rate of movement in an ensemble of filaments, electron microscopy measures the extent, or amplitude of this movement in in-

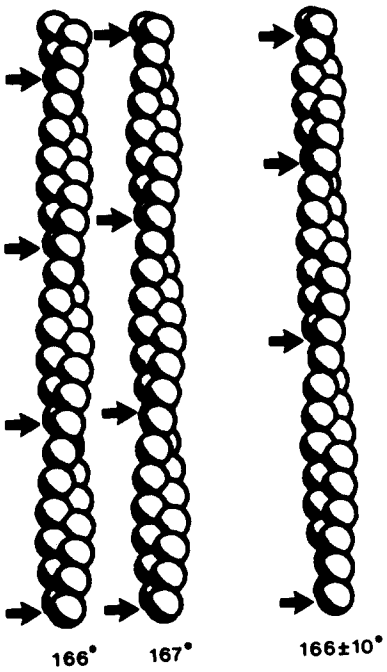

Figure 1. Diagram depicting variable twist. Each sphere represents an actin subunit, and the subunits have been helically arranged to form both ordered (*left*) and disordered (*right*) filaments. The two filaments on the left have been constructed with a fixed angle between subunits of 166 and 167°, as indicated. The filament on the right has been constructed with a variable angle between subunits; the RMS deviation of 10° per subunit has been allowed to accumulate from one subunit to the next, thereby generating cumulative angular disorder. This disorder gives rise to a variable twist along the actin filament as well as to a variability in the distance between crossovers (*arrows*).

dividual filaments that have been fixed in time. It seems plausible that these two different kinds of measurements both derive from thermally induced variations in the twist of the actin filaments, which in turn result from random deviations in the angular positions of individual subunits.

Electron microscopic evidence for the existence of this variable twist in actin began with the observations of Hanson (1967). She noticed a variability in the distance between crossovers on single actin filaments, but she did not provide a structural interpretation for her observations. Many years later, Egelman et al. (1982) provided this interpretation by hypothesizing an accumulation of disorder in the angular positions of actin subunits; the effects of this disorder on the appearance of an actin filament are depicted in Fig. 1. The disorder, called cumulative angular disorder, accounts not only for the variability in crossover distances, but also for the variability in the twist of actin filaments, for a systematic attenuation of layer line intensities in Fourier transforms, and for a variability in the distance between filaments in an Mg^{++}-induced network of actin filaments, called the angle-layered aggregate. Egelman et al. (1982) considered the experimental evidence for all of these effects, and they estimated that single actin filaments have a variability of ~10° in the angle between subunits. This variability is sufficient to account for the 7° of twisting required to cross-bridge filaments into actin bundles. Considering the large binding energy between actin and myosin, this variability may also be sufficient to account for the distortions observed in the reconstructions of insect flight muscle.

While some assemblies appear to make use of variable twist, the function of the actin bundle from *Limulus* sperm appears to require filaments that are rather inflexible with regard to twisting. This bundle is a part of the acrosomal process, and is composed of actin and an actin-binding protein called scruin. Initially, the bulk of the bundle is coiled about the base of the sperm. Upon contact of the sperm with an egg cell, the bundle uncoils and extends some 60 μm out of the anterior end of the sperm cell. A change in the twist of the actin filaments of <1° per subunit causes this extension of the bundle (DeRosier et al., 1982). Since the twist is so tightly controlled, we wondered if individual, isolated filaments from this bundle would have a reduced variability in twist.

Such considerations led us to further characterize the variable twist of actin and to measure this variability in several different actin-containing filaments. To do so, we implemented two independent methods for measuring the cumulative angular disorder, or variable twist, of isolated filaments. One is based on layer line position and the second on layer line intensity as a function of filament length. We used both methods to analyze actin filaments that were preserved in three different ways: in negative stain, in replicas of freeze-etched filaments, and in the frozen hydrated state. We also studied three other actin-containing filaments: actin bound to tropomyosin (Tm)[1] and troponin (Tn), the calcium regulatory proteins in striated muscle; actin bound to subfragment 1 (S1) of myosin, the force-generating protein from muscle; and individual filaments frayed from the bundle of

1. *Abbreviations used in this paper*: S1, subfragment of myosin; Tm, tropomyosin; Tn, troponin.

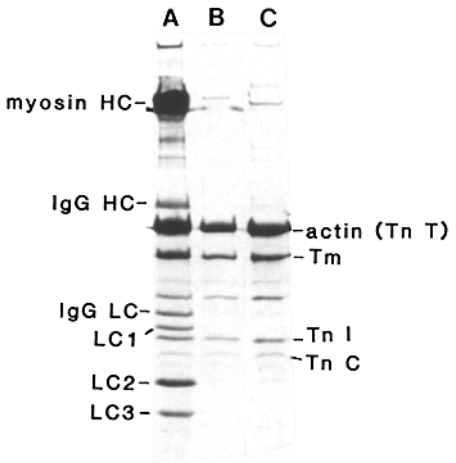

Figure 2. Gel electrophoresis of preparations of actin + Tm + Tn. The preparation and the gel were provided by Don Winkelmann (UMDNS-Robert Wood Johnson Medical School, Piscataway, NJ). Lane *A* represents the entire myofibril after addition of a monoclonal antibody to myosin. The addition of the antibody causes aggregation of the A bands, which can then be removed by centrifugation. Lane *B* represents the supernatant after precipitation of the A band. The filaments in the supernatant were collected by further centrifugation and run in lane *C*. The gel shows that the preparation contains actin, Tm, Tn, and IgG heavy and light chains, as well as some other unidentified components that may come from the Z disk. HC, heavy chain; LC, light chain; LC1, 2, and 3, myosin light chains.

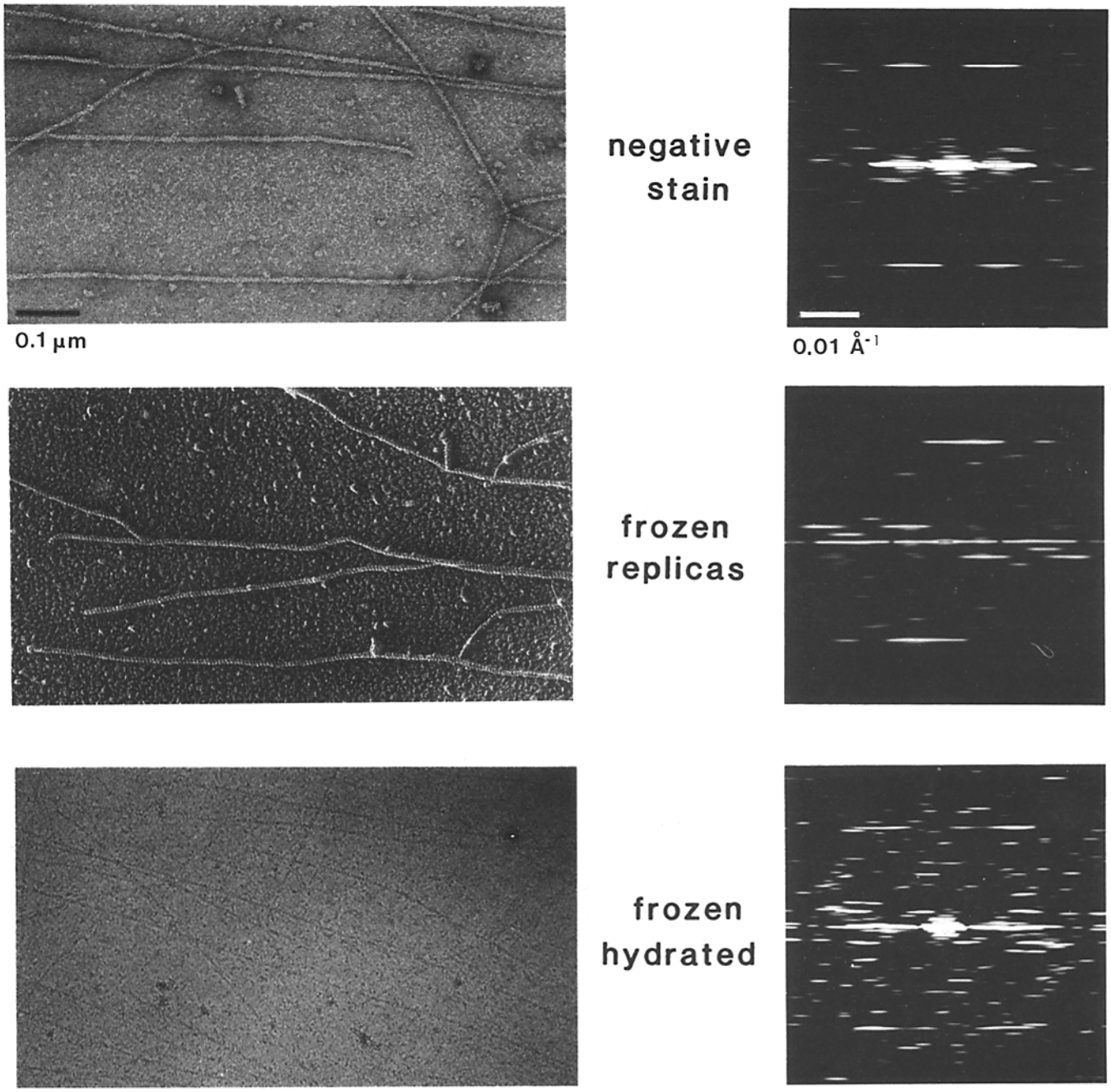

Figure 3. Micrographs of three preparations of actin filaments and Fourier transforms of corresponding single filaments. Transforms were computed from single filaments that were digitized and masked (see Materials and Methods). The larger diameter of frozen replicated filaments results from metal accumulation during shadowing, while the low, reversed contrast is characteristic of images of frozen hydrated filaments. Each Fourier transform is dominated by layer lines at 1/360 $Å^{-1}$ (first) and at 1/59 $Å^{-1}$ (sixth, see Fig. 7 for identification). The transform from frozen replicated filaments is asymmetric (i.e., one-sided) because the replicas contain information from only one side of the filaments.

Limulus sperm, which are thought to contain actin and the bundling protein, scruin. Since we detected comparable quantities of cumulative angular disorder in negatively stained and in frozen preparations of actin filaments, this disorder cannot be an artefact of negative stain nor of adsorption to a support film. We suggest that the disorder corresponds to the torsional mobility of actin filaments seen in solution. We found that actin + Tm + Tn had a variability similar to actin's, but that actin + S1 and *Limulus* filaments had very little variability. The preservation of this variability in twist by Tm + Tn probably reflects the need to accommodate symmetry mismatches in striated muscle. The reduced variability in twist in *Limulus* filaments may reflect the tight control over actin's twist, since small changes in twist are associated with the exposive extension of the bundle in *Limulus* sperm.

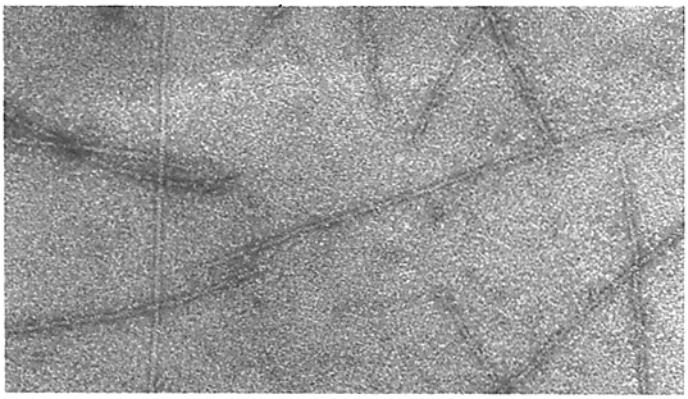

actin
+ Tm
+ Tn

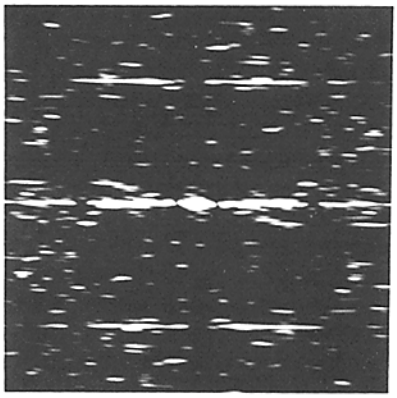

0.1 μm

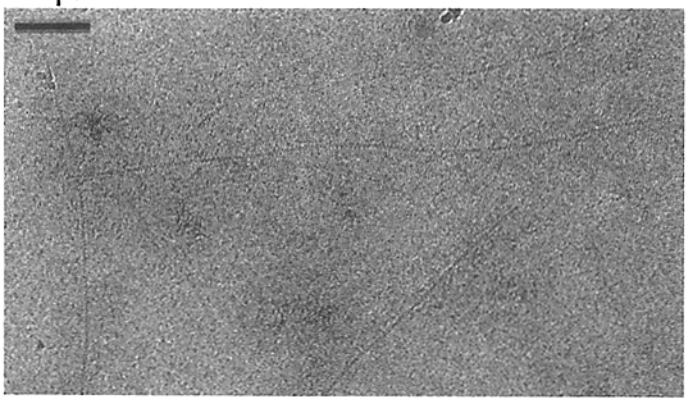

frozen
hydrated
actin
+ Tm
+ Tn

0.01 Å^{-1}

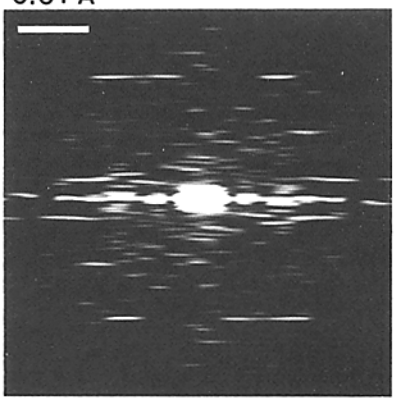

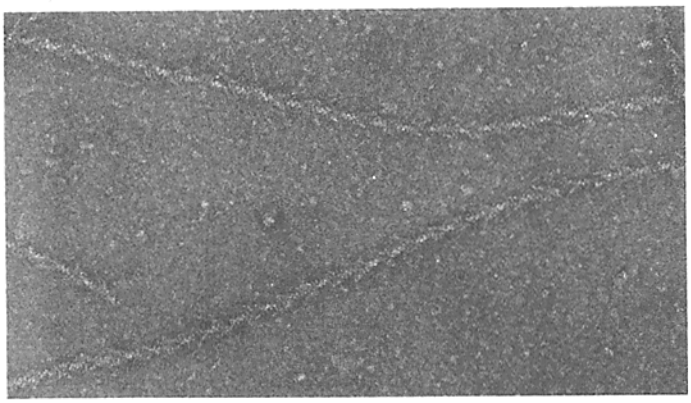

actin
+ S1

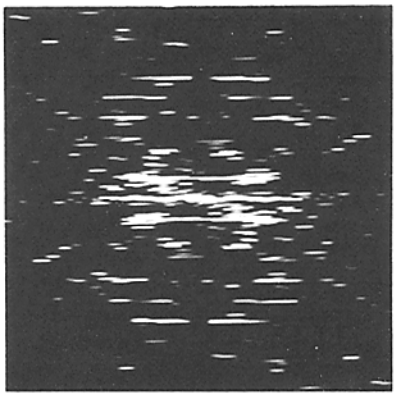

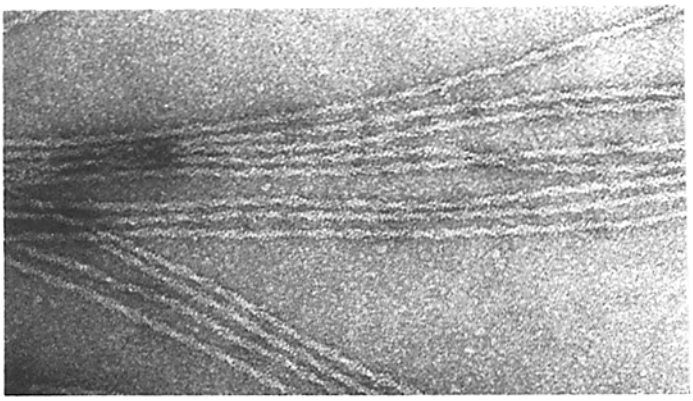

Limulus
filaments

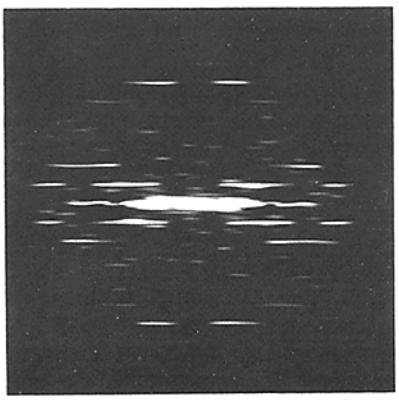

Materials and Methods

Specimen Preparation

The actin used for negative staining was extracted from chicken pectoralis muscle, while the actin used both for freeze-etch replicas and for frozen hydrated microscopy was extracted from rabbit psoas muscle. All actin was extracted into an acetone powder by the standard method of Spudich and Watt (1971) and later reconstituted for electron microscopy.

Filaments of actin + Tm + Tn which were used for negative staining were extracted directly from chicken pectoralis muscle by the method of J. L. Woodhead, S. Lowey, and D. A. Winkelmann (personal communication). Briefly, this method involves separating the A band from the I band with a monoclonal antibody to myosin S1 in a low ionic strength relaxing buffer. The cross-linked thick filaments were removed by centrifugation, leaving the I band in the supernatant. Filaments of actin + Tm + Tn were finally collected from this supernatant by centrifugation. Gel electrophoresis confirmed that all three proteins were present in the final preparation of filaments (Fig. 2). Filaments of actin + Tm + Tn which were used for frozen hydrated microscopy were extracted from glycerinated rabbit psoas muscle by the method of Kendrick-Jones et al. (1970). Unbuffered Ca^{++} was present in both preparations of filaments.

Myosin S1 was prepared by treating myosin, isolated from the A band, with papain (2% myosin was treated with 15 μg/ml papain for 7–10 min [Rayment and Winkelmann, 1984]). The decoration of actin with myosin S1 was then performed directly on the electron microscopy grid. A molar ratio of actin subunits to S1 of approximately 1:1 both minimized background in micrographs and maximized decoration of actin by myosin S1.

Filaments from the acrosomal process of *Limulus* sperm were frayed directly from these actin bundles and micrographs were taken (E. S. A. Bullitt, D. J. DeRosier, L. Coluccio, and L. G. Tilney, personal communication). Acrosomal processes, isolated from sperm after treatment with 1% Triton X-100 according to Tilney (1975), were frayed by treatment either with 0.5 M KSCN for 4–15 min or with 0.8 M KI for up to 8 min. (Longer times resulted in complete solubilization of the processes.) After treatment, processes were put on electron microscopy grids, washed with buffer several times, and negatively stained with 1–2% uranyl acetate. Single filaments from the frayed ends were photographed and were later used in the analysis.

It has not yet been possible to isolate the frayed filaments and thereby to determine their composition directly, but structural analysis of micrographs suggests a 1:1 ratio of scruin to actin. The native bundle consists of actin and scruin in equimolar ratio (Tilney, 1975). The 95-kD protein, originally thought to be part of the bundle, now appears to be associated with a contaminating structure from the acrosomal vacuole (Y. Fukui, L. G. Tilney, and R. Goldman, personal communication). The bundle, as seen in negatively stained preparations, consists of hexagonally packed filaments separated by ~100Å (DeRosier et al., 1977). Negative stain, however, was found to cause shrinkage, and the true interfilament spacing in bundles is 140–150 Å (DeRosier and Tilney, 1984). Three-dimensional reconstructions from electron micrographs of negatively stained bundles show filaments ~100Å in diameter which have two outer morphological features (DeRosier et al., 1977). If these reconstructions are corrected for shrinkage, they are very similar to three-dimensional reconstructions done recently from the frayed filaments, which have the same diameter of 150Å and the same two outer morphological domains (E. S. A. Bullitt, D. J. DeRosier, L. Coluccio, and L. G. Tilney, personal communication). The higher radial resolution of the reconstructions from frayed filaments allows identification of three morphological domains in all, two of which closely resemble in size, shape, and position the two domains of the actin subunit that were proposed by Egelman et al. (1983). The third domain, which is at the largest radius of the three, has been assigned as the bound scruin subunit and is within 10% of the volume expected for this 55-kD protein. In summary, two structural observations suggest that the frayed filaments contain actin and scruin: (*a*) the similarity between the reconstructions of filaments from intact and from frayed bundles and (*b*) the similarity between the inner two domains of the reconstructions and the proposed structure for actin.

Electron Microscopy

To negatively stain preparations, filaments and frayed bundles were allowed to adsorb for ~1 min onto a thin carbon film that covered an electron microscopy grid. The grids were then washed with buffer, stained with 1% uranyl acetate, and allowed to air dry. All negatively stained preparations were photographed in a Philips EM 301 at 57,000× with an accelerating voltage of 80 kV. Typical micrographs of actin filaments are shown in Fig. 3 together with a Fourier transform of a single filament; micrographs and transforms of other actin-containing filaments are shown in Fig. 4.

Replicas of freeze-etched actin filaments were prepared and photographed by John Heuser (Washington University School of Medicine, St. Louis, MO), who was kind enough to lend us the micrographs. These filaments were adsorbed onto mica, and then frozen by plunging the specimen onto a copper block, which was cooled by liquid He. The frozen filaments were etched at ~180°K in a Balzers freeze fracture device (Balzers, Hudson, NH) and rotary shadowed at a low angle with Pt/C. The Pt/C replicas were then photographed in the electron microscope at 65,000× and at 100 kV (Heuser, 1983).

With the technique of frozen hydrated microscopy (Dubochet et al., 1982), micrographs of actin and of actin + Tm + Tn were obtained by P. Flicker (University of California, Berkeley, CA) and R. Milligan (Stanford University, Stanford, CA), who were also kind enough to lend us these micrographs. Filaments were placed onto a grid covered by holey Formvar films. The grid was then quickly blotted between two pieces of filter paper and plunged into liquid ethane, which was cooled by liquid N_2. The grids were stored in liquid N_2 until they were transferred to the electron microscope (Gatan Cryotransfer System model 626 or Philips PW 6500/00 cryoholder). Once in the microscope (Philips EM 400), grids were kept at ~100°K, and filaments that were suspended over holes in vitreous ice were photographed at 33,000–43,000× at 100 kV with 1.6–2.2 μm defocus.

Theory of Cumulative Angular Disorder

A mathematical derivation of the effects of cumulative angular disorder on actin structure and on Fourier transforms of actin has been published elsewhere (Egelman and DeRosier, 1982). We will review those aspects of the theory that are relevant to our quantification of angular disorder in actin filaments. This quantification involves two kinds of measurements: (*a*) the variance of a distribution of helical twists for a set of filaments of equal length, and (*b*) the variation of layer line intensity as a function of filament length.

The geometry of the actin filament is depicted in Fig. 5. According to the analysis of Egelman and DeRosier (1982), the angular position of a given subunit relative to its immediate neighbors is variable, giving rise to deviations in the angle between subunits ($\Delta\Phi$). In the case of cumulative angular disorder, these deviations add up as one moves along the helix, so that the total angular deviation after N subunits equals the sum of the individual deviations from each subunit. In contrast, the deviations do not add for noncumulative disorder, so that the total deviation after N subunits would simply equal the deviation of the Nth subunit. In addition to these two types of angular disorder, there could also exist both cumulative and noncumulative axial disorder, where the error is in the axial position (z) of subunits.

Effect of Disorder on Filament Twist. Any of these four types of disorder will produce a variability in crossover spacings, as originally observed by Hanson (1967). However, only angular disorders will produce a variability in actin's twist. A distribution of twist measurements, therefore, will be affected by the presence of angular, but not of axial disorder. To derive these effects, we first define the variance ($\langle \Delta s^2 \rangle$) of a group of twist measurements (s_j) as

$$\langle \Delta s^2 \rangle = \langle (s_j - \bar{s})^2 \rangle, \quad (1)$$

where $\bar{s}$ is the mean twist expressed as the number of subunits in one turn

Figure 4. Micrographs of three actin-containing filaments and Fourier transforms of corresponding single filaments. Filaments of actin + Tm + Tn have a similar diameter to actin (90 Å), while actin + S1 filaments (200 Å) and *Limulus* filaments (150 Å) are wider. The low, reversed contrast of frozen hydrated filaments is typical of the technique. Transforms of actin + Tm + Tn are similar to those of actin and are dominated by layer lines 1 and 6. Actin + S1 and *Limulus* filaments produce other layer lines (4, 5, and 7 for actin + S1 and 2, 5, and 7 for *Limulus* filaments). The presence of additional layer lines can be explained both by the increased helical order of these filaments and by the different morphology of these filaments.

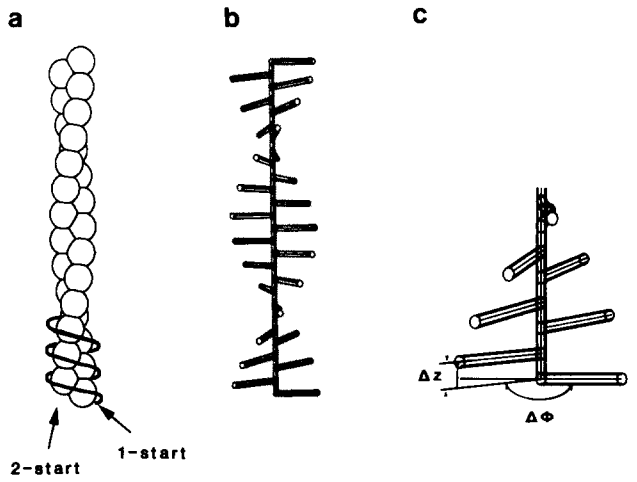

Figure 5. Geometry of the actin filament. A filament is schematically drawn in *a*; actin monomers are represented as spheres. The one-start helix, sometimes called the genetic helix, has a pitch of 59 Å and gives rise to the sixth layer line in Fourier transforms; the helical twist of actin can be expressed as the number of subunits in one turn of this one-start helix, usually ~2.16. The two-start helix has a pitch of ~360 Å and gives rise to the first layer line in Fourier transforms. In *b*, the spherical subunits have been replaced by thin rods to illustrate the angular orientation of the subunits. In *c* the first few subunits have been magnified to show two parameters, which together completely describe the helix: the angle ($\Delta\Phi$) and the axial rise (Δz) between subunits along the one-start helix. While z remains invariant, $\Delta\Phi$ varies from one subunit to the next. This variability gives rise to cumulative angular disorder.

of the 59-Å, one-start helix (see Fig. 1). Each twist measurement (s_j) can be expressed in terms of the total angle (Φ_j) traversed by this one-start helix after N subunits:

$$s_j = 2\pi N/\Phi_j. \quad (2)$$

Cumulative angular disorder will, in general, perturb the value for Φ_j as follows:

$$\Phi_j = N\bar{\Phi} + N^{1/2}d_{rms}, \quad (3)$$

where $\bar{\Phi}$ is the average angle between adjacent subunits and d_{rms} is the amount of cumulative angular disorder, expressed as the root mean square (rms) angular deviation per subunit (Egelman and DeRosier, 1982). If one substitutes Eq. 3 into Eq. 2, and then substitutes Eq. 2 into Eq. 1, the result can be rearranged to yield

$$\langle \Delta s^2 \rangle^{1/2} = \bar{s}^2 d_{rms}/2\ N^{1/2} \quad (4)$$

by assuming that $d_{rms}/(\bar{\Phi}\ N^{1/2}) << 1$. This assumption implies either that the rms deviation of a subunit is considerably less than the angle between subunits, or that the filaments under consideration are composed of many subunits; both of these conditions are met in our analysis of actin filaments $d_{rms}/(\bar{\Phi}N^{1/2}) = 0.3/(3 \times 10) = 0.01$. The derivation of the effects of noncumulative angular disorder is analogous except that Eq. 3 is replaced by

$$\Phi_j = N\bar{\Phi} + d_{rms}. \quad (5)$$

The resulting distribution of helical twists is characterized by the right side of Eq. 4 divided by $N^{1/2}$. Note therefore, that the distribution for noncumulative angular disorder depends on N^{-1}, while that for cumulative angular disorder depends on $N^{-1/2}$. These results imply that for a filament of reasonable length (e.g., N = 100), noncumulative angular disorder will have 10-fold less effect than cumulative angular disorder on these distributions of twist.

Effect of Disorder on Layer Line Intensity. All four types of disorder will also affect layer line intensities of Fourier transforms from single filaments, but only the effects of cumulative disorders on layer line intensity are length dependent. Noncumulative disorders are analogous to a crystallographic temperature factor, which simply dampens intensity at higher resolution; this dampening is independent of filament length. Cumulative disorders, however, systematically reduce the rate of increase of layer line intensities as a function of filament length. The reduction in rate depends both on the amount of disorder and either on the Bessel order (n) for angular disorder, or on the distance of the layer line from the equator (Z) for axial disorder. This particular dependence provides a sensitive method for quantifying cumulative disorders from the ratio of layer line intensities. In addition, this method is independent of any noncumulative disorders.

The dependence of the intensity ratio of a layer line ($I(n,Z)$) on cumulative angular disorder has been derived as

$$I(n,Z) = 8I^\circ/(d_{rms}n)^4\ (Nn^2d_{rms}^2/2 - 1 + e^{-Nn^2d_{rms}^2/2}), \quad (6)$$

where d_{rms} is the amount of angular disorder, and I° is the intensity in the absence of disorder (Egelman and DeRosier, 1982). Our analysis of actin filaments has quantified only cumulative angular disorder, but we have derived the effects of cumulative axial disorder to be able to recognize these effects should this disorder be present. The derivation for cumulative axial disorder is analogous to that for cumulative angular disorder, yielding:

$$I(n,Z) = 8I^\circ/(\zeta_{rms}2\pi Z)^4[N(2\pi Z\zeta_{rms})^2/2 - 1 + e^{-N(2\pi Z\zeta_{rms})^2/2}] \quad (7)$$

where ζ_{rms} is the amount of axial disorder, expressed as the rms axial deviation per subunit. Eq. 7 is equivalent to Eq. 6 except that (nd_{rms}) has been replaced by ($2\pi Z\zeta_{rms}$).

By measuring the intensities of two layer lines with different values for n and Z as a function of filament length, one can assess the amount of cumulative angular, or cumulative axial disorder, in these filaments. The use of the ratio of layer line intensities eliminates many of the problems inherent in directly comparing intensities from different images. Fig. 6 illustrates the effects both of cumulative angular and of cumulative axial disorder on the intensity ratio of layer line 1 (n_1 = 2, Z_1 = 1/360 Å^{-1}) to layer line 6 (n_6 = −1, Z_6 = 1/59 Å^{-1}) from a Fourier transform of an actin filament. The y intercept of each curve represents the intensity ratio in the absence of disorder (Y°). The asymptotic limit at infinite filament length (Y^∞) is determined either by the Bessel orders (i.e., $Y^\infty/Y^\circ = (n_6/n_1)^2$ = 1/4) or by the axial heights (i.e., $Y^\infty/Y^\circ = (Z_6/Z_1)^2$ = 36) of the layer lines under consideration. The rate at which these asymptotic limits are approached depends on the amount of disorder. For this particular pair of layer lines, cumulative angular disorder has an effect on the intensity ratios that is opposite

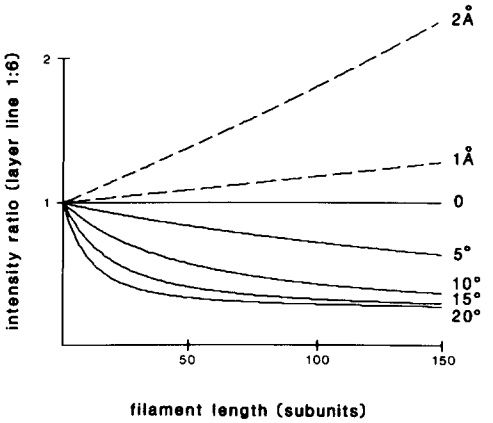

Figure 6. Theoretical effects of cumulative angular and of cumulative axial disorder on intensity ratios from Fourier transforms. The intensity ratio of layer line 1/layer line 6 as a function of filament length has been calculated according to Eqs. 6 (for angular disorder) and 7 (for axial disorder). The intensity ratio in the absence of disorder (Y° corresponding to the y intercept) has arbitrarily been taken as 1. The flat curve corresponds to a constant intensity ratio in the absence of either type of cumulative disorder. Upward, dashed curves correspond to 1 and 2 Å of cumulative axial disorder, and, downward, solid curves correspond to 5, 10, 15, and 20° of cumulative angular disorder. Both sets of curves tend toward asymptotic limits at infinite filament lengths (Y^∞ = 1/4 for angular and 36 for axial disorder). These limits are easily seen for large amounts of angular disorder (e.g., 15°), but the scale of this graph masks the limits for axial disorder, the curves for which are still in their linear phases.

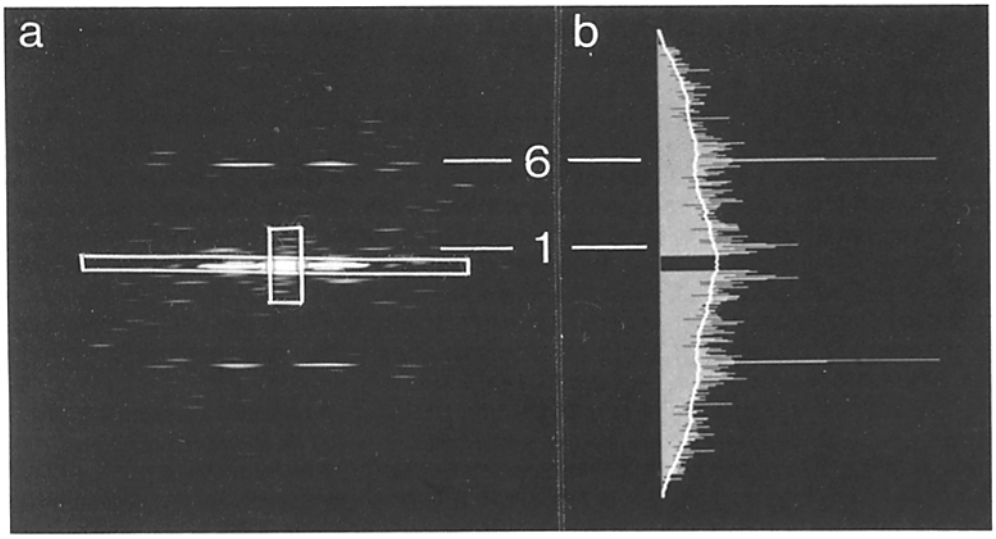

Figure 7. Measurement of layer lines from Fourier transforms. A two-dimensional Fourier transform from a negatively stained actin filament is shown in *a*. The intensities from this transform have been integrated along horizontal lines to produce the projection in *b*; the length of each line in *b* corresponds to the magnitude of this integrated intensity. The intensity within the white boxes shown on the transform were excluded from the projection; the low order meridional intensity was masked off to prevent its contribution to the first layer line, and the equator was excluded for convenience. Layer line 1 (at 1/360 $Å^{-1}$) and layer line 6 (at 1/59 $Å^{-1}$) are marked and are clearly visible both in the transform and in its projection. The solid white line across the projection represents the background, calculated from a portion of the micrograph adjacent to the actin filament. This background was scaled and then subtracted from the projection before measuring the integrated intensities and the positions of the two layer lines.

from cumulative axial disorder. The curve for cumulative axial disorder in the range shown in Fig. 6 is still very far from its asymptotic limit and hence appears linear.

It is relatively easy to derive the corresponding expressions for layer line intensity in the presence of noncumulative disorders. The expressions are

$$I(n,Z) = I°N^2\,(1 - n^2 d_{rms}^2/2)^2 \text{ for angular disorder} \quad (8)$$

and

$$I(n,Z) = I°N^2\,(1 - (2\pi Z\zeta_{rms})^2/2)^2 \text{ for axial disorder.} \quad (9)$$

When ratios of intensities from two different layer lines are taken, the dependence on length (i.e., N^2) cancels.

Digital Fourier Analysis

We used a computer (VAX 11/780) to determine both layer line positions and layer line intensities from Fourier transforms of single actin filaments. From these two types of measurements, we determined the amount of cumulative angular disorder present in these filaments. Since the positions of the layer lines, used to calculate twist, are independent from the intensities, the two determinations of disorder are independent of one another. The analyses began by digitizing (P1000 rotary scanner; Optronics, Inc., Chelmsford, MA) between 15 and 35 images of each filament type. The images were sampled at 50-μm intervals, corresponding to a 9-Å sampling of the negatively stained filaments, 11-Å sampling for frozen replicated filaments, and 12–15 Å for frozen hydrated filaments. Each filament image was then cut into overlapping segments that were 2, 3, 4, 6, 8, and 10 crossovers in length, and a 512 by 512 point Fourier transform of each segment was calculated as described by DeRosier and Moore (1970). Fig. 7 illustrates the projection of one such Fourier transform onto the meridional axis and identifies the background in this projection. This background was calculated from a part of the micrograph that was devoid of filaments and that was directly adjacent to the filament under consideration. The background image was Fourier transformed and projected; the projected background was then scaled to achieve the best fit to the projections from each segment of the filament. After subtracting this background from each projection, both the helical twist and the intensity ratio of layer line 1 (1/360 $Å^{-1}$) to layer line 6 (1/59 $Å^{-1}$) were measured. The twist, s, of the filament was calculated as:

$$s = 2 + Z_1/Z_6, \quad (10)$$

where Z_i is the distance of layer line i from the equator (DeRosier and Censullo, 1981). The values for Z_1 and Z_6 were obtained by fitting the three points spanning each projected peak by a curve of the form

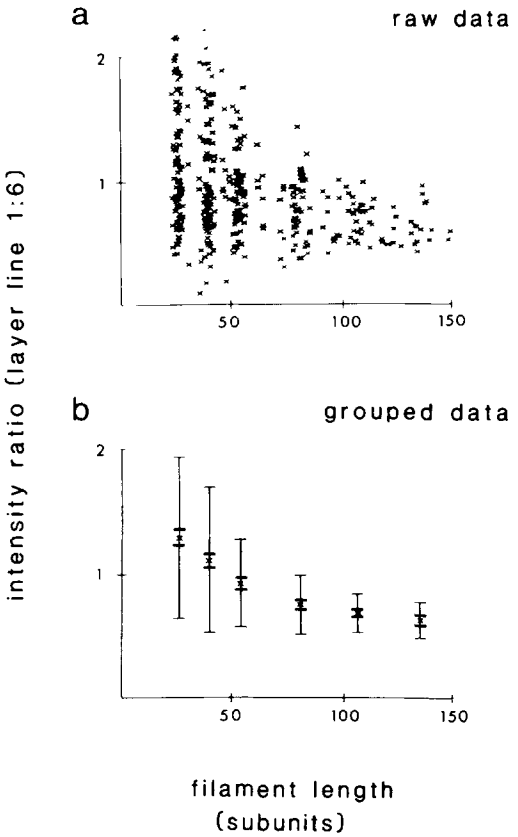

Figure 8. The grouping of intensity ratio data. The points in *a* represent individual measurements of intensity ratio from segments of negatively stained actin filaments, normalized as described in the text. These data have been grouped according to filament length: 20–35, 35–50, 50–70, 70–90, 90–120, and above 120 subunits. In *b*, the average intensity ratio has been plotted versus the average length of the group. The large error bars represent the standard deviation, and the small error bars represent the standard error of the mean of the group.

$$y = ax^2 + bx + c.$$

The position of the peak is given by $x = -b/2a$, and the intensity of the peak is given by $-b^2/4a + c$. Intensity ratios of layer lines 1 to 6 were computed and normalized (see below).

To estimate the amount of cumulative angular disorder from helical twists, as calculated from layer line positions, a distribution of twist measurements was accumulated. All filaments in a given data set were of a uniform length, corresponding to ~90 subunits. The standard deviation of each of these distributions of twist reflects the amount of cumulative angular disorder, d_{rms}, according to Eq. 4. The standard error of this standard deviation can be calculated as $\sigma/\sqrt{2n}$, where σ is the standard deviation and n is the number of filaments in the distribution. By using Eq. 4, this standard error can be translated into the standard error of d_{rms}; the 95% confidence interval can then be defined as $d_{rms} \pm 2$ SEM.

To estimate the amount of cumulative angular disorder from layer line intensities, it was necessary to normalize intensity ratios, since peculiarities in stain distribution (e.g., positive staining, one-sided staining [Trus and Steven, 1984]) or differences in defocus will change the absolute intensity ratios. For a given filament, normalization was accomplished by dividing observed intensity ratios by the average intensity ratio from all segments from that filament. We used this average value because any single measurement is more subject to noise and therefore is less reliable. Because it is a linear correction, this normalization will not affect the rate of decrease of the intensity ratio with filament length; rather, it will place ratios from many different filaments on the same scale. The normalized intensity ratios of the first to the sixth layer line were plotted as a function of filament length (Fig. 8 *a*). The data were grouped according to filament length and the means of each group are plotted in Fig. 8 *b*. The large error bars represent the standard deviation, while the small error bars represent the standard error of the mean. We then fit Eq. 6 to the averaged data, thereby determining the two parameters in this equation: the rms angular deviation (d_{rms}) and the normalized intensity ratio in the absence of disorder ($Y°$, corresponding to the y intercept). We used a χ^2 statistical test to determine the best fit and to determine the range of acceptable fits. The χ^2 statistic is calculated as

$$\chi^2 = \sum_{i=1}^{6} (Y_i - Y_{theory})^2/\sigma_i^2$$

where Y_i are the six means in Fig. 8 *b*, σ_i are the associated standard errors, and Y_{theory} are the theoretical values for the intensity ratio based on d_{rms}, $Y°$, and filament length. The values of d_{rms} and $Y°$ that yield the minimum value for χ^2 (χ^2_{min}) represent the best fit to the data. Given the six data points (i.e., the six means), two constants to be fit (i.e., d_{rms} and $Y°$), and the normalization of intensity data, which removes one degree of freedom, the number of degrees of freedom is 3; therefore, the expectation value for χ^2_{min} is 3. Experimental measures of χ^2_{min} are not expected to exceed 7.8 (95% confidence) if data are fit by theory to within experimental error (i.e., σ^2). Since we are fitting curves having two parameters, d_{rms} and $Y°$, the 95% confidence limits for these two parameters are defined by $\chi^2_{min} + 6$ (Meyer, 1975). By calculating χ^2 for a range of theoretical curves, we can determine the values of d_{rms} and $Y°$ that produce $\chi^2_{min} + 6$ and thereby determine a statistically significant range of values for d_{rms} and $Y°$.

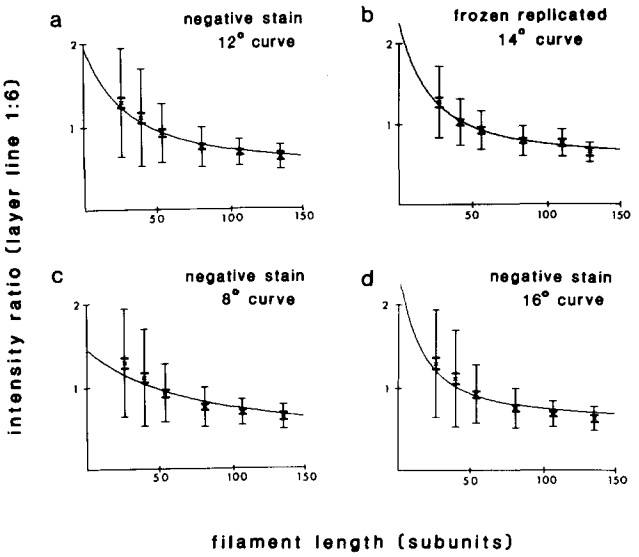

Figure 9. Fitting of theoretical curves to the data both from negatively stained and from frozen replicated actin filaments. Data are grouped as in Fig. 4, both with standard errors and with standard deviations indicated. The curves drawn in *a* and *b* represent the best fit for negatively stained ($Y° = 1.95$, $d_{rms} = 12°$) and for frozen replicated ($Y° = 2.25$, $d_{rms} = 14°$) filaments. The curves in *c* ($Y° = 1.45$, $d_{rms} = 8°$) and in *d* ($Y° = 2.4$, $d_{rms} = 16°$) lie just outside the 95% confidence interval as determined by χ^2 analysis (see Fig. 11). Clearly, these curves do not fit the data for negatively stained filaments as well as the curve in *a*.

Results

Actin

We used intensity ratios of layer line 1 to layer line 6, measured as a function of filament length, to quantify cumulative angular disorder, or variable twist, in actin filaments. These intensity ratios are plotted in Fig. 9 for negatively stained and for frozen replicated filaments of actin. A similar plot could not be made for frozen hydrated actin due to the low electron dose used to photograph these filaments; the resulting images had a weak signal, preventing reliable measurement of intensity ratios at lengths shorter than about six crossovers.

The smooth curves in Fig. 9 represent the theoretical relationship between intensity ratio and filament length (Eq. 6). Each curve is characterized by the amount of cumulative angular disorder, d_{rms}, and by the intensity ratio in the absence of disorder, $Y°$. The data have been pooled such that each point in Fig. 9 represents the average of data from filament segments of approximately equal length; the large error bars represent the standard deviation, and the small error bars the standard error of the mean. According to our χ^2 analysis, a curve with $d_{rms} = 11.5°$ and $Y° = 1.85$ fits the data from negatively stained filaments best with a range of $d_{rms} = 8.5$–$15°$ and $Y° = 1.5$–2.2 (95% confidence interval). This analysis is illustrated in Fig. 10, which is a plot of χ^2 as a function of both d_{rms} and $Y°$. The x marks the values of d_{rms} and $Y°$ that produce a minimum value of χ^2 (χ^2_{min}) and

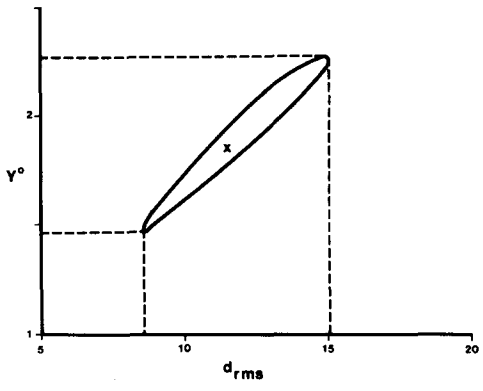

Figure 10. χ^2 fitting of theoretical curves to intensity ratio data. This contour plot represents the value of χ^2 (described in text) as a function of $Y°$ and d_{rms}. The x represents the minimum value of χ^2 (in this case 3.9) and the single contour represents $\chi^2_{min} + 6$ (in this case 9.9). According to χ^2 analysis, the upper right and lower left edges of this elliptical contour represent the range of values for $Y°$ and d_{rms} (95% confidence interval). To obtain a different confidence interval, one would draw a contour at a different value for χ^2 (e.g., 99% confidence interval defined by $\chi^2_{min} + 9.2$).

Table I. Amount of Cumulative Angular Disorder in Actin-containing Filaments

Filament type	d_{rms} from intensity ratios			d_{rms} from twist measurements	
	Best value (degree)	Range* (degree)	χ^2_{min}	Best value (degree)	Range* (degree)
Negatively stained actin	11.5	8.5–14.0	3.9	13.5	10.2–16.7
Frozen replicated actin	14.0	7.2–18.2	2.4	9.6	6.6–12.6
Frozen hydrated actin	–	–	–	11.6	8.9–14.3
Negatively stained actin + Tm + Tn	18.0	8.0–23.0	0.1	14.2	10.6–17.8
Frozen hydrated actin + Tm + Tn	–	–	–	13.7	9.1–18.3
Negatively stained actin + S1	0.5	0.0–2.3	2.6	3.6	2.4–4.8
Negatively stained *Limulus* filaments	0.0	0.0–3.8	1.2	1.9	1.3–2.5

* The range represents the 95% confidence interval determined from the χ^2 analysis as $\chi^2_{min} + 6$ or from the distributions of twist as two times the standard error of d_{rms}.

therefore the best fit for the data. Since there are 3 degrees of freedom, the measured value of χ^2_{min} should exceed 7.8 only 5% of the time; the observed value of 3.9 therefore indicates that the data are fit by theoretical curves to within our experimental error (see Materials and Methods). The ellipse encompasses a range of values that produce $\chi^2 < \chi^2_{min} + 6$. The angle of the major axis of this ellipse reflects the covariance of d_{rms} with $Y°$. The upper right and lower left edges of the ellipse define the 95% confidence intervals for d_{rms} and $Y°$ (i.e., d_{rms} = 8.5–15° and $Y°$ = 1.5–2.2). These confidence intervals are depicted in Figs. 9 *c* and *d*; they show theoretical curves corresponding to 8 and 16° of disorder, which lie just outside the 95% confidence intervals set by χ^2 analysis. We have carried out the identical analysis for intensity data from frozen replicated filaments; these data are best fit by d_{rms} = 14.0° and $Y°$ = 2.25 (Fig. 9 *b*) with a range of d_{rms} = 7.25–18.25° (results tabulated in Table I).

In an independent set of measurements, we used layer line position instead of intensity to quantify cumulative angular disorder in these same actin filaments. The frequencies with which particular values of twist occur are shown in Fig. 11 for negatively stained actin, for frozen replicated actin, and for frozen hydrated actin. The amount of disorder can be obtained from the standard deviation of each distribution according to Eq. 4. The error associated with the standard deviation, and hence with the amount of disorder, is described in Materials and Methods. The resulting values for d_{rms} and the 95% confidence intervals are shown in Table I. These values agree well with each other and with those from the intensity ratio data; that is, the means from the five different populations of measurements from actin filaments show no significant differences. The simple average of all the means is 12° with a range of ~8.4–15.6° (corresponding to a standard deviation of 1.8°).

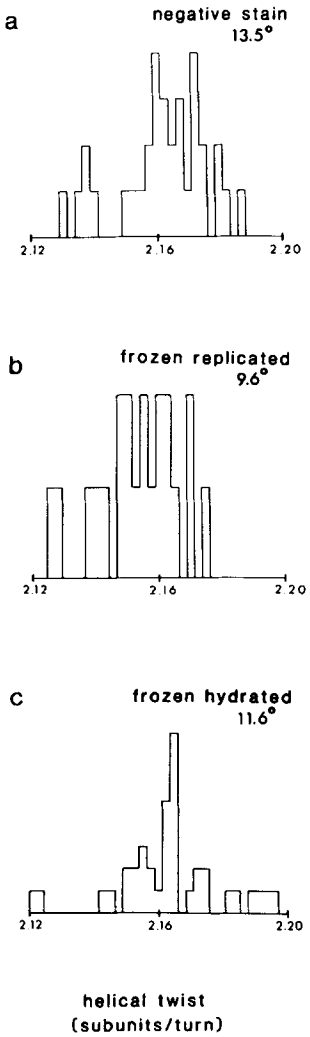

Figure 11. Distributions of helical twist in the three preparations of actin filaments. The standard deviation of each of these distributions can be directly related to the amount of cumulative angular disorder according to Eq. 4. *a* contains data from 33 negatively stained filaments, with an average length of 102 subunits. This distribution has a standard deviation of 0.0172 corresponding to d_{rms} = 13.5°. *b* contains data from 21 frozen replicated filaments with an average length of 88 subunits; the standard deviation of 0.0133 corresponds to d_{rms} = 9.6°. *c* contains data from 37 frozen hydrated filaments with an average length of 98 subunits; the standard deviation of 0.0158 corresponds to d_{rms} = 11.6°.

Actin-binding Proteins

Actin-binding proteins mediate the interactions within actin assemblies and may use actin's variable twist in different ways, depending on the function of their respective assemblies. Therefore, we measured the effect of several actin-binding proteins on the amount of cumulative angular disorder in actin filaments. Three types of actin-containing filaments were measured: actin + Tm + Tn + Ca^{++}, actin + myosin S1, and filaments from the acrosomal process of *Limulus* sperm. The intensity ratio data from negatively stained filaments are plotted in Fig. 12 and can be compared with analogous data for actin that are plotted in Fig. 9. A similar plot could not be derived from micrographs of frozen hydrated actin + Tm + Tn, due to a low signal/noise ratio at moderate and at short filament lengths. Notice that the data both from actin (Fig. 9) and from actin + Tm + Tn (Fig. 12 *a*) have distinct curvature, while the data from actin + S1 (Fig. 12 *b*) and from *Limulus* filaments (Fig. 12 *c*) have no

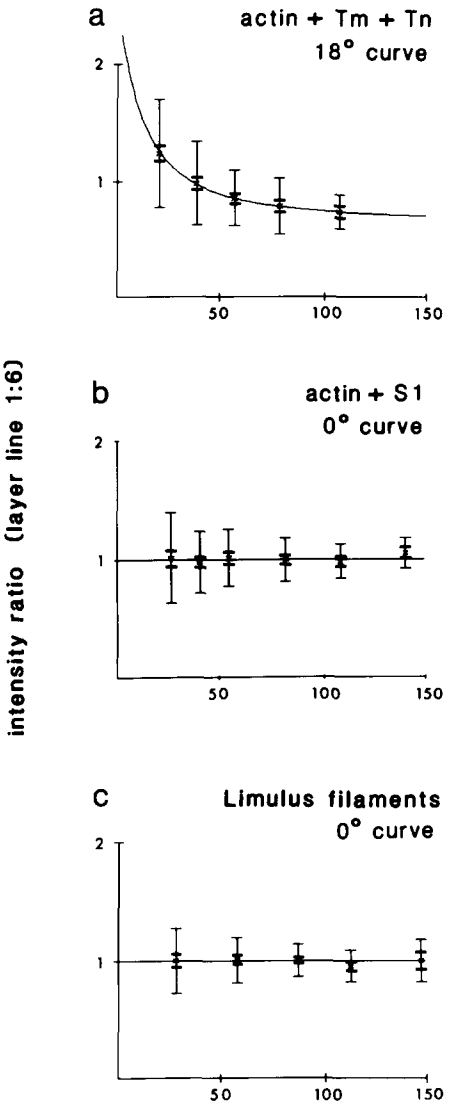

Figure 12. Measurement of angular disorder in actin-containing filaments from plots of intensity ratio versus filament length. Data are plotted as in Figs. 4 and 9. The smooth lines drawn through the data represent the theoretical curves that, according to χ^2 analysis, best fit the data. The parameters used to draw each curve are as follows: actin + Tm + Tn, d_{rms} = 18°, $Y°$ = 2.5; actin + S1, d_{rms} = 0°, $Y°$ = 1.0; actin + *Limulus* protein, d_{rms} = 0°, $Y°$ = 1.0.

detectable curvature. This indicates that, like actin, filaments of actin + Tm + Tn have considerable cumulative angular disorder, while both actin + S1 filaments and *Limulus* filaments have little, if any, disorder. χ^2 analysis corroborates these observations, the results of which are listed in Table I.

In a second, independent measure of angular disorder, we measured distributions of helical twist for these three types of filaments. The histograms resulting from these measurements are shown in Fig. 13 and can be compared with the analogous data for actin in Fig. 11. There is a broad distribution of twists, both from negatively stained actin (Fig. 11 *a*) and from actin + Tm + Tn (Fig. 13 *a*), as well as from frozen hydrated filaments of actin + Tm + Tn (Fig. 13 *b*). In contrast, the distributions derived from actin + S1 and from *Limulus* filaments demonstrate considerably less variability (Fig. 13, *c* and *d*). The corresponding values for d_{rms} are listed in Table I.

The agreement between d_{rms} determined from layer line position and from layer line intensity is excellent except for actin + S1 (Table I). In this case both estimates for d_{rms} are small, but the 3.6° measured from layer line position is significantly larger than that measured from layer line intensities. Since for small values of d_{rms} (i.e., from actin + S1 and *Limulus* filaments) the estimates derived from layer line position were larger than those derived from intensities, we considered the possibility that errors in measurement of layer line position might be adding to the variance in distributions of twist. The total variance of the observed twist distribution will equal the sum of the individual variances from disorder and from measurement error, because the variation in twist due to measurement error is independent of that due to angular disorder. An increased variance will increase our estimate of d_{rms}; thus, errors in layer line position, unlike those in intensity, will systematically increase d_{rms}.

To estimate the error associated with each measurement of helical twist, we chose one or more typical images from each type of filament and repeatedly measured its twist (i.e.,

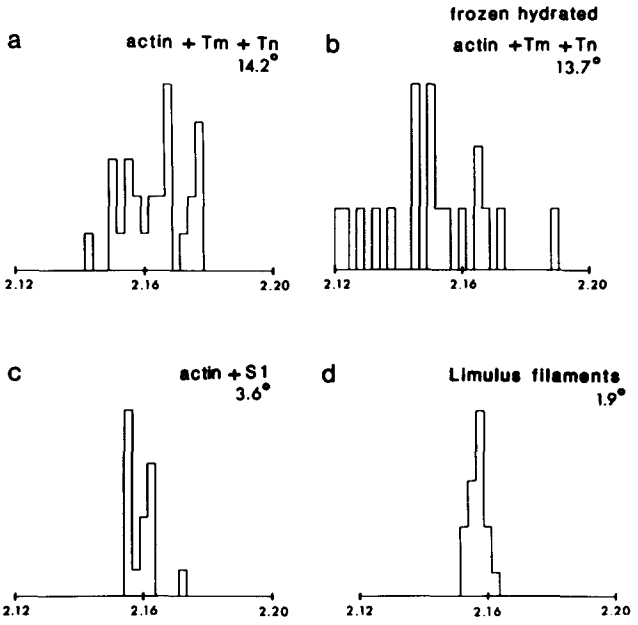

Figure 13. Measurement of angular disorder in actin-containing filaments from the distribution of twist. The standard deviation of each distribution is linearly related to the amount of cumulative angular disorder according to Eq. 4. The number of observations (n), the standard deviation (s), the number of subunits in each filament (N), and the corresponding amount of cumulative angular disorder (d_{rms}) are as follows: actin + Tm + Tn, n = 31, s = 0.0219, N = 71, d_{rms} = 14.2°; frozen hydrated actin + Tm + Tn, n = 19, s = 0.0169, N = 108, d_{rms} = 13.7°; actin + S1, n = 17, s = 0.0045, N = 109, d_{rms} = 3.6°; *Limulus* filaments, n = 20, s = 0.00254, N = 92, d_{rms} = 1.9°.

redigitized, remasked, retransformed, and remeasured the layer line positions). From the standard deviation of the repeated measurements (e.g., 0.0037 for negatively stained actin), we determined the measurement error in units of d_{rms}. Thus we calculated a measurement error of 2.8° for actin, 3.0° for actin + Tm + Tn, 0.6° for actin + S1, and 0.2° for *Limulus* filaments. A value for angular disorder from twist measurements can be obtained by subtracting the variance due to error (corresponding to $2.8°^2$ in actin filaments) from the variance of the observed distribution ($13°^2$ in actin filaments): $(13^2 - 2.8^2)^{1/2} = 12.7°$. So considered, the observed measurement errors reduce the estimates of disorder from twist distributions very little (i.e., the estimates of disorder in actin + S1 and *Limulus* filaments are reduced by <0.1°, and in actin and actin + Tm + Tn by ~0.3°). Therefore, the difference in our estimates of disorder for actin + S1 must arise from other sources.

Discussion

The Variable Twist of Actin

We have measured variability in the twist of several actin-containing filaments and now make several general observations regarding these measurements. First, we used two independent measures of variable twist and the results were in good agreement. In the case of intensity ratio data, statistical analysis indicated that these data were well fit by theoretical curves to within experimental error. Second, there were no statistically significant differences between the values for d_{rms} from negatively stained, frozen replicated, and frozen hydrated actin filaments. These results indicate that variable twist is not an artefact of negative stain nor of adsorption to a carbon film. This was also suggested by Trinick et al. (1986), who observed a variability in the distance between actin's crossovers in filtered images of frozen hydrated filaments; they did not attempt to quantify this variability. Third, we also measured variable twist in actin + Tm + Tn, both negatively stained and frozen hydrated. Although the mean value for actin + Tm + Tn is higher than that for pure actin, the difference is not significant. Fourth, little variable twist was measured in actin + S1 and in *Limulus* filaments, and the means for both types of filaments were significantly less than those for pure actin or for actin + Tm + Tn.

We have considered four types of disorder, and we have evidence that cumulative angular disorder is the dominant form of disorder. Two lines of reasoning suggest that cumulative axial disorder is very small in actin. First, the lack of any upward trend in the plots of intensity ratio at long filament lengths, which are very sensitive to small amounts of this disorder (see Fig. 6), indicates that cumulative axial disorder must be <1 Å per subunit. Second, the distributions of filament twist give estimates of angular disorder that are comparable to those obtained from the intensity ratio curves. If there were a significant amount of cumulative axial disorder, it would reduce the rate at which the intensity ratio declines with filament length. This can be visualized by simply combining two of the curves in Fig. 6, one for angular and one for axial disorder. Assuming the existence of cumulative angular disorder only, the resulting curve would lead to an underestimate of the amount of this disorder. The distributions of twist, however, would remain unchanged or become slightly broader in the presence of axial disorder, as indicated by studies on simulated actin filaments (unpublished observations). In this case, the resulting distribution would lead to an overestimate of the amount of angular disorder. Since our estimates from these independent methods are about the same, we conclude that cumulative axial disorder is small in actin filaments. We have also considered noncumulative axial and noncumulative angular disorders. However, our measurements are not sensitive to these disorders since (*a*) they would produce no variation in intensity ratio with length, and (*b*) they would have about a 10-fold smaller effect on distributions of twist (see Materials and Methods). Hence, we cannot rule out the presence of noncumulative disorders, but we can eliminate them as an explanation for our results.

We have considered the effects of several potential artefacts, both on the intensities and on the positions of layer lines in Fourier transforms, and have thereby eliminated each of their effects from our analyses. First, interference between adjacent layer lines, which results from the finite length of the images, can easily be eliminated by using filament segments corresponding to an integral number of repeats, e.g., 2, 3, 4, 6, 8, 10 crossovers (DeRosier and Moore, 1970). Since the intensity ratio curve was unaffected by the use of random filament lengths (data not shown), this interference appears to be insignificant. Second, the contribution to the first layer line from meridional noise near the central maximum was eliminated by excluding the meridian from the projection of the Fourier transform (see Fig. 7). Third, the background was determined from areas of the micrographs immediately adjacent to each filament image; this background was then subtracted from the projection of each Fourier transform (see Fig. 7). Fourth, the effect of filament curvature was minimized by using only the straightest filaments. Even when a small amount of curvature is present, it does not produce the observed effects, either on layer line intensity or on layer line position (Egelman and DeRosier, unpublished observations). Fifth, one-sided staining of filaments and differences in defocus of images are compensated for by the normalization of intensity ratios (see Materials and Methods). A difficulty could arise if, for example, the 1-start helical grooves were evenly stained but the 2-start grooves progressed from light to heavy staining along the length of the filament. This particular situation would produce systematic changes in layer line intensity along the filament and would result in a decrease in the intensity ratio as a function of length. Since examination of short (two crossovers) consecutive stretches from each filament did not suggest such trends in stain distribution, this effect does not explain the observed decline of intensity ratio with length.

Torsional Flexibility in Solution

We think that the angular disorder intrinsic to electron micrographs of actin filaments is caused by a dynamic torsional flexibility of these filaments in solution. An alternative view is of an actin filament with some built-in static disorder, but there are two other lines of evidence that support the notion of a dynamic flexibility. First, the original studies of cumulative angular disorder by Egelman et al. (1983) included an analysis of Mg^{++}-induced angle-layered aggregates of actin filaments. These aggregates are formed from two layers

of parallel filaments at an oblique angle to one another. The filaments in one layer are bonded to the filaments in the other layer approximately at their crossovers; thus the observed variability in the distance between filaments within one layer indicates variability in crossover spacings of the filaments in the other layer. The key point is that in order to form a network of bonded filaments, all filaments in a layer must be disordered in exactly the same way. Thus, to bond to the growing aggregate, actin filaments must be able to vary their twist until it matches that of the existing aggregate. The energy required for the twisting is supplied by the bonding energy of the filaments in the assembly.

A second line of evidence for dynamic twisting of actin comes from two spectroscopic studies that indicate a dynamic mobility with a time constant of ~0.1–0.5 ms. Thomas et al. (1979) make a strong case for the immobility of their electron magnetic resonance probe, and, therefore, for their observations being due to "an internal rotational mode of F-actin." Yoshimura et al. (1984) are even more specific in their assignment of this mobility to a torsional flexibility that is "compatible . . . with the variable twist of the F-actin helix." They also apply a nonlinear mathematical formulation (Barkley and Zimm, 1979) of restricted torsional motion to their measurements of optical anisotropy, and thereby calculate a mean angular displacement of 4.3° per actin subunit. In this calculation they encounter several problems, such as (*a*) the mobility of their probe relative to actin, (*b*) a discrepancy between the initial value for anisotropy measured and that predicted by theory, and (*c*) the nonlinear relationship both of the probe orientation and of the mean angular displacement to the data. Furthermore, this formulation assumes a particular force–displacement relationship (that of a harmonic oscillator), which may not be applicable to actin. Considering these potential problems, their smaller value cannot be taken as inconsistent with our results. Rather, the most important aspect of their work, and of that by Thomas et al., is the evidence for a torsional mobility of actin in solution.

Taken together, the electron microscopic and spectroscopic work both on the angular disorder and on the torsional mobility of actin show that the actin subunits can bond at different angles in the filament. There is no information about the distribution of angles between pairs of subunits. At one extreme, the angle could vary freely, as if there were hinges within or between subunits. At the other extreme, there could be only two possible bonding angles corresponding to two possible conformational states of the subunit. The hinged model corresponds to quasi-equivalent bonding in which flexibility within a polymeric protein assembly results from variation in bonding angle (Caspar and Klug, 1962). At the other extreme, the two-state model corresponds to a rigid bonding in which variability occurs by subunit switching (Monod et al., 1965). Both models are observed in nature, and it remains to be discovered which best describes the variability in actin.

Actin-binding Proteins

Our results show that actin + S1 and *Limulus* filaments have little or no cumulative angular disorder, indicating that the variability in actin's twist is essentially eliminated. Our results also indicate that the presence of Tm + Tn maintain, or perhaps enhance this disorder. The effects of these actin-binding proteins on actin's cumulative angular disorder, and therefore on actin's torsional flexibility, must reflect the structural interactions between the proteins. Since these interactions determine the biological properties of the filaments, our observations of disorder are likely to reflect the functioning of the various actin assemblies.

Tropomyosin and Troponin. The preservation of actin's cumulative angular disorder by Tm + Tn may reflect the need for torsional flexibility in the functioning of striated muscle fibers. The helical symmetries of thick (myosin) and thin (actin + Tn + Tm) filaments in striated muscle are different, and neither is compatible with the hexagonal filament lattice (Huxley and Brown, 1967). Therefore, some sort of flexibility is needed in order to accommodate the force-generating interactions between the two types of filaments. This flexibility could be satisfied by the hinges in the myosin molecule, and/or by the torsional flexibility of the thin filament. Evidence for the flexibility of thin filaments comes from a three-dimensional reconstruction of insect flight muscle during rigor (Taylor et al., 1984). In addition to distortions of the myosin molecules, this reconstruction reveals a striking untwisting and a compensatory overtwisting of the actin helix, which are associated with myosin binding. This observation supports the notion that actin's torsional flexibility is used to resolve these mismatches in symmetry.

There is independent evidence regarding the specific amount of torsional flexibility in thin filaments relative to actin. Our measurements indicate that Tm + Tn maintain the magnitude of angular disorder (see Table I). Spectroscopic sources indicate that thin filaments in solution have slightly lower torsional mobilities than actin filaments (Thomas et al., 1979; Mihashi et al., 1983). It is difficult to directly compare the electron microscopic measurements with those derived from spectroscopy, since angular disorder measured by microscopy reflects the extent of the motion and spectroscopy measures rates of motion. However, assuming the torsional motion to be like a harmonic oscillator, Mihashi et al. (1983) calculated a 20% increase in the force constant of thin filaments relative to actin. If we adopt the hypothesis of harmonic motion, the data of Mihashi et al. would predict a 20% decrease in the disorder of thin filaments relative to actin. This would correspond to an expected value of $\sim 0.8 \times 12 = 9.6° \pm 0.8 \times 3.6 = 2.8°$ (corresponding to two standard deviations). The measured means of 18.0, 14.2, and 13.7 average to 15.3° ± 4.8°. According to Student's *t* test, this difference is significant at the 99% level. A resolution of this discrepancy must await a more thorough understanding of the structural basis for actin's flexibility.

Myosin S1. There are two distinct explanations for the dramatic reduction of actin's angular disorder by myosin S1. First, the bond between actin and S1 might directly restrict actin's torsional mobility. This restriction could arise either by altering the conformation of actin in a way that restricts its rotational hinge, or by binding a single S1 molecule across this rotational hinge, either within a subunit or between two subunits. Second, as has been suggested by Egelman (1985), the reduction of angular disorder by S1 might indirectly arise from steric hindrance between adjacent S1 molecules along actin's two-start helix. However, two independent spectroscopic studies of actin's rotational mobilities (Thomas et al., 1979; Yoshimura et al., 1984), which probably cor-

respond to our measurements of angular disorder, have reported that low ratios of S1 to actin (e.g., 1:10) cause a large reduction in this mobility. If there is in fact reduced mobility at such low ratios, it probably is not caused by steric interaction between neighboring S1 molecules, but by a direct effect of S1 on the flexibility of the actin filament.

The biological relevance of an actin + S1 filament with reduced torsional flexibility is unclear. In fact, the electron microscopic observations of large angular distortions during rigor in insect flight muscle (Taylor et al., 1984) seem, at first, to conflict with the notion of a torsionally stiffer actin + S1 filament. It seems clear that some flexibility is necessary to produce the observed distortions, and we have already referred to them as evidence for a flexible thin filament. These distortions probably reflect the geometrical constraints of a hexagonal lattice on actin's helical symmetry. If the binding of myosin to actin does in fact stiffen the thin filament, the effect of such stiffening will be to increase the amount of energy needed to maintain the angular distortions. This energy could be compensated by the formation of actin–myosin bonds, and might play some unforeseen role in force transduction.

Limulus-bundling Protein (Scruin). The reduced angular disorder in filaments frayed from the acrosomal process of *Limulus* sperm may very well be important for the biological function of this actin bundle from these sperm. Recall that the bundle undergoes a dramatic extension, which is driven by a twist change in the component filaments of <1° per subunit (DeRosier et al., 1982). It has been suggested that this twist change is mediated by a control system within the bundle itself, e.g., scruin (DeRosier and Tilney, 1984). If so, scruin may also restrict the angular flexibility of individual filaments, thereby accounting for our results. We do not know, however, if it is indeed scruin that reduces the angular disorder. It could be that this species of actin has low disorder or even that treatment of the bundle with KSCN reduces the disorder. In any case, it would not be surprising that a system that tightly controls the twist of its actin filaments in vivo would also reduce the variability in twist of individual actin filaments in vitro.

We thank John Heuser for providing us with micrographs of frozen replicated actin, Paula Flicker and Ron Milligan for micrographs of frozen hydrated actin and actin + Tm + Tn, Peter Vibert for micrographs of actin + S1, and Don Winkelmann for solutions of thin filaments and of S1. We also thank Petr Honcu and Judith Black for photography.

This work was supported by National Institutes of Health grant GM26357. D. L. Stokes was supported by National Institutes of Health training grant 2T32GM07596.

Received for publication 19 June 1986, and in revised form 3 November 1986.

References

Barkley, M. D., and B. H. Zimm. 1979. Theory of twisting and bending of chain macromolecules: analysis of the fluorescence depolarization of DNA. *J. Chem. Phys.* 70: 2991–3007.

Caspar, D. L. D., and A. Klug. 1962. Physical principles in the construction of regular viruses. *Cold Spring Harbor Symp. Quant. Biol.* 27:1–24.

DeRosier, D. J., and P. B. Moore. 1970. Reconstruction of three-dimensional images from electron micrographs of structures with helical symmetry. *J. Mol. Biol.* 52:355–369.

DeRosier, D., E. Mandelkow, A. Silliman, L. Tilney, and R. Kane. 1977. Structure of actin-containing filaments from two types of non-muscle cells. *J. Mol. Biol.* 113:679–695.

DeRosier, D. J., and R. Censullo. 1981. Structure of f-actin needles from extracts of sea urchin oocytes. *J. Mol. Biol.* 146:77–99.

DeRosier, D. J., L. G. Tilney, E. M. Bonder, and P. Frankl. 1982. A change in twist of actin provides the force for the extension of the acrosomal process in *Limulus* sperm: the false-discharge reaction. *J. Cell Biol.* 93: 324–337.

DeRosier, D. J., and L. G. Tilney. 1984. The form and function of actin: a product of its unique design. *In* Cell and Muscle Motility. Vol. 5. J. W. Shay, editor. Plenum Publishing Corp., New York. 139–169.

Dubochet, J., J. Lepault, R. Freeman, J. A. Berriman, J.-C. Homo. 1982. Electron microscopy of frozen water and aqueous solutions. *J. Microsc. (Paris).* 128:219–237.

Egelman, E. H., and D. J. DeRosier. 1982. The fourier transform of actin and other helical systems with cumulative random angular disorder. *Acta Crystallogr. Sect. B Struct. Crystallogr. Cryst. Chem.* A38:796–799.

Egelman, E. H., N. Francis, and D. J. DeRosier. 1982. F-actin is a helix with a random variable twist. *Nature (Lond.).* 298:131–135.

Egelman, E. H., N. Francis, and D. J. DeRosier. 1983. Helical disorder and the filament structure of f-actin are elucidated by the angle-layered aggregate. *J. Mol. Biol.* 116:605–629.

Egelman, E. H. 1985. The structure of f-actin. *J. Muscle Res. Cell Motil.* 6:129–151.

Hanson, J. 1967. Axial period of actin filaments. *Nature (Lond.).* 213:353–356.

Heuser, J. 1983. Procedure for freeze-drying molecules adsorbed to mica flakes. *J. Mol. Biol.* 169:155–195.

Huxley, H. E., and W. Brown. 1967. The low-angle x-ray diagram of vertebrate striated muscle and its behavior during contraction and rigor. *J. Mol. Biol.* 30:383–434.

Kendrick-Jones, J., W. Lehman, and A. G. Szent-Györgyi. 1970. Regulation of molluscan muscles. *J. Mol. Biol.* 54:313–326.

Meyer, S. L. 1975. Data Analysis for Scientists and Engineers. John Wiley and Sons Inc., New York. pp. 254–273, 359–386.

Mihashi, K., H. Yoshimura, T. Nishio, A. Ikegami, and K. Kinosita, Jr. 1983. Internal motion of f-actin in 10^{-6}–10^{-3} s time range studied by transient absorption anisotropy: detection of torsional motion. *J. Biochem.* 93:1705–1707.

Monod, J., J. Wyman, and J.-P. Changeux. 1965. On the nature of allosteric transitions: a plausible model. *J. Mol. Biol.* 12:88–118.

Rayment, I., and D. A. Winkelmann. 1984. Crystallization of myosin subfragment 1. *Proc. Natl. Acad. Sci. USA.* 81:4378–4380.

Spudich, J. A., and S. Watt. 1971. The regulation of rabbit skeletal muscle contraction. *J. Biol. Chem.* 246:4866–4871.

Taylor, K. A., M. C. Reedy, L. Córdova, and M. K. Reedy. 1984. Three dimensional reconstruction of rigor insect flight muscle from tilted thin sections. *Nature (Lond.).* 310:285–291.

Thomas, D. D., J. C. Seidel, and J. Gergely. 1979. Rotational dynamics of spin-labeled f-actin in the sub-millisecond time range. *J. Mol. Biol.* 132: 257–273.

Tilney, L. G. 1975. Actin filaments in the acrosomal process of *Limulus* sperm. *J. Cell Biol.* 64:289–310.

Trinick, J., J. Cooper, J. Seymour, and E. H. Egelman. 1986. Cryo-electron microscopy and three-dimensional reconstruction of actin filaments. *J. Microsc. (Paris).* 141:349–360.

Trus, B. L., and A. C. Steven. 1984. Diffraction patterns from stained and unstained helices: consistency or contradiction? *Ultramicroscopy.* 15:325–336.

Yoshimura, H., T. Nishio, and K. Mihashi. 1984. Torsional motion of eosin-labeled f-actin as detected in time-resolved anisotropy decay of the probe in the sub-millisecond time range. *J. Mol. Biol.* 179:453–467.